Proceedings of the ASME 2015 Dynamic Systems and Control Conference
DSCC2015
October 28-30, 2015 Columbus, Ohio, USA

DSCC2015-9636

ACTIVE AND PASSIVE VIBRATION CONTROL USING COMPACT DAMPING PATCHES: ASSESSMENT OF A REDUCED ORDER MODEL FOR AN EULER BEAM

Joseph Plattenburg
The Ohio State University
Columbus, OH, USA

Jason T. Dreyer
The Ohio State University
Columbus, OH, USA

Rajendra Singh
The Ohio State University
Columbus, OH, USA

ABSTRACT

Concurrent placement of compact active and passive damping patches for vibration reduction is a developing area of research. Analytical and computational models to evaluate alternate patch configurations and structural geometries are not widely available. To overcome this void, this paper presents a simplified discrete-system model for vibrations of a beam-like structure. A disturbance input is included in the model, along with a control input from an active patch. Localized structural damping resulting from a passive patch is modeled with an equivalent loss factor. Results from the simplified model are verified using a more detailed analytical formulation, which is based on the Ritz approximation. Verification studies include the effect of a passive damping patch on modal loss factors and broadband attenuation. Finally, a few case studies are proposed which show the efficacy of the reduced-order model for parametric design studies. These studies include determining the effect of localized damping on the control system parameters that are required for attenuation of localized and global motions. The effect of patch locations on system response is also studied. This work has potential applications in industry since compact damping patches are attractive NVH treatments that add minimal weight and complexity.

1 INTRODUCTION

The combination of active and passive noise and vibration reduction techniques is an emerging area of research with applications in many industries such as automotive and aerospace [1]. Kung and Singh [2, 3] developed a model based on the Rayleigh-Ritz method for thin beams and plates with constrained layer passive patches containing a viscoelastic core. Piezoelectric active patches on beams and plates were studied by Clark et al. [4] and Dimitriadis et al. [5], respectively, using the modal expansion approach. One of the first attempts to analytically examine compact active and passive damping patches together in a "side-by-side" configuration was carried out by Lam et al. [6] using a Ritz-Galerkin method. Their method seeks to complement active control with increased structural damping. Most studies consider flexural motion of the base structure (i.e. beam, plate, etc.) where passive patches act to induce larger modal loss factors [2, 3] and active patches introduce motion to enact destructive interference [7], as shown in Fig. 1(a). Much of the existing literature cited here utilizes analytical continuous-system methods or finite element formulations. A more detailed literature review of this area is available in [3] and [7].

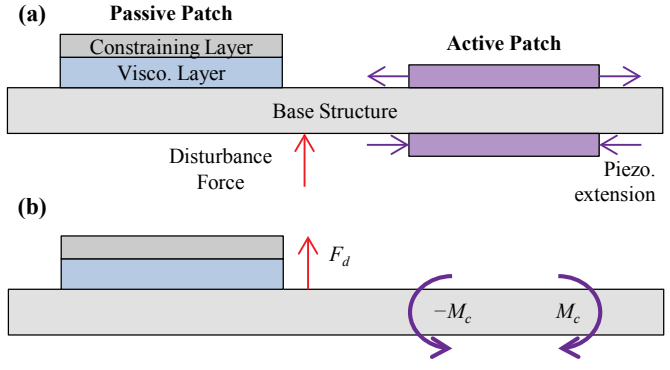

Figure 1. Beam-like structure of interest: (a) generic placement of passive patch and active patch pair in the side-by-side configuration; (b) equivalent (positive convention) loading from active patch and disturbance

2 PROBLEM FORMULATION

Comprehensive models are needed to predict and evaluate attenuation characteristics for combined patch configurations. High-level finite element codes [8] and detailed analytical formulations [3, 5, 7] are valuable for predicting accurate results; however the complexity of these formulations may not clearly illustrate underlying phenomena and trends. As such, the objectives of this paper are as follows. (1) Develop a reduced-order (i.e. discretized-system) model of an Euler beam with active and passive damping patches. (2) Verify that this model (designated M2) gives reasonable results as compared to a more accurate continuous-system model (designated M1). (3) Utilize the proposed reduced-order model to efficiently conduct studies and gain insight. Proposed studies include determining trends in how passive patch placement effects active control and structural response of the beam. An overview of the two models is included in Table 1.

Table 1. Alternate proposed damping patch models

Model Name	Description	Method	Dimension/ Complexity
M1	Semi-Analytical Plate with Multiple Damping Patches	Rayleigh-Ritz	2-D Structure, Multiple Layers, Continuous System Formulation
M2	Computational Beam with Equivalent Structural Damping	Finite Element	1-D Structure, Single Layer, Discretized System Formulation (2 degrees-of-freedom per node)

Model M1 assumes a rectangular plate with multi-layered passive damping patches (as described in Section 3) and input from active patches. For the scope of this paper, the plate will be assumed to behave like a beam by considering a large length-to-width ratio (i.e. $L_x >> L_y$). Conversely, M2 will assume only a single layer for passive patch/base structure system but will also be restricted to one-dimensional beam geometry. Equations of motion are derived in the time domain using energy principles and Newtonian formulation, but analyses will be restricted to the frequency domain by assuming steady-state harmonic response. The base structure material is assumed to have (negligible) structural damping in the form of a loss factor, η_1, as is the passive patch viscoelastic material, η_2 (with $\eta_2 >> \eta_1$). Only free boundaries for the Euler beam are considered for this study, and excitation frequency will be limited to selected resonant modes. Furthermore, the system is assumed to be linear and time-invariant (i.e. system matrices are time-invariant), allowing for application of the principle of superposition. Finally, active patches negligibly affect the mass and stiffness distribution of the structure and are used only in "bimorph" pair configurations (as in Fig. 1(a)) with perfect adhesion, resulting in a moment input.

3 CONTINUOUS SYSTEM MODEL (M1)

Kung and Singh [3] developed an analytical model, following the Rayleigh-Ritz approximation, for the out-of-plane vibratory motion of a plate with passive constrained layer damping patches. This model is extended to include the addition of multiple active patches (detailed derivation can be found from Plattenburg et al. [7]) as follows. Consider a rectangular plate (layer 1) having dimension $L_x \times L_y$, with constrained layer damping patches consisting of a viscoelastic adhesive layer and elastic constraining layer (layers 2 and 3, respectively). The motions of the three individual layers of an infinitesimal element are shown in the *xz* plane in Fig. 2, and consist of transverse flexural motion, w, in-plane motions u and v (in the x and y directions, respectively), and rotations ψ_x and ψ_y (in the *xz* and *yz* planes, respectively). Motions in the *yz* plane are analogous, with v replacing u and y replacing x. Layer i has thickness h_i, as well as material properties E_i (Young's modulus), ρ_i (density), η_i (loss factor), and ν_i (Poisson's ratio); sample material properties are given in Table 2. Note that w is assumed identical for all three layers and shear is neglected in layers 1 and 3 (thus $\psi_{x1} = \psi_{x3} = \partial w/\partial x$, etc.)

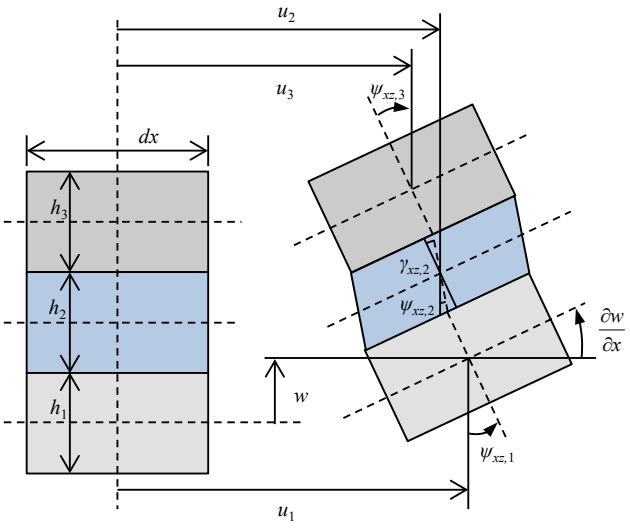

Figure 2. Motions of all layers in the *xz* plane: undeformed element, left, vs. deformed element, right (adapted from [3])

The kinetic (K) and potential (U) energy for the plate and corresponding patches can be written as follows [9]:

$$K = \frac{1}{2}\sum_{i=1}^{3}\iint_{A_i}\rho_i h_i\left(\dot{w}^2 + \dot{u}_i^2 + \dot{v}_i^2\right)dxdy, \tag{1a}$$

$$\begin{aligned} U = \frac{1}{2}\sum_{i=1}^{3}\Bigg\{ & \iint_{A_i}\frac{E_i h_i^3}{12\left(1-\nu_i^2\right)}\left(w_{xx}^2 + w_{yy}^2 + \ldots\right. \\ & \left. 2\nu_i w_{xx}w_{yy} + 2\left(1-\nu_i\right)w_{xy}^2\right)dxdy + \ldots \\ & \iint_{A_i}\frac{E_i h_i}{\left(1-\nu_i^2\right)}\left(u_{ix}^2 + v_{iy}^2 + 2\nu_i u_{ix}v_{iy} + \ldots\right. \\ & \left.\frac{\left(1-\nu_i\right)}{2}\left(v_{ix} + u_{iy}\right)^2 + \frac{\left(1-\nu_i\right)}{2}\left(\gamma_{ix}^2 + \gamma_{iy}^2\right)\right)dxdy\Bigg\}. \end{aligned} \tag{1b}$$

Here, summations are over layers i = 1–3; integrals are over area of the i^{th} layer, A_i; γ is shear strain, with $\gamma_1 = \gamma_3 = 0$ and $\gamma_{xz,2} = (\partial w/\partial x - \psi_{xz,2})$, etc.; and subscripts x and y (i.e. w_{xx}) refer to spatial partial derivatives.

Table 2. Selected material and geometric properties

M1 Model Properties (Fig. 2)			
Property	**Layer 1**	**Layer 2**	**Layer 3**
Material	Aluminum	Adhesive	Steel
Young's Modulus, E [GPa]	70	0.018	203
Density, ρ [kg/m^3]	2700	730	7800
Loss Factor, η	0.001	2.0	0.005
Poisson's Ratio, ν	0.33	0.4	0.3
Thickness, h [mm]	10.0	0.9	0.5
M2 Properties (Fig. 4c)			
Property	**Base Element**	**Patch Element**	
Young's Modulus, E [GPa]	70	70	
Density, ρ [kg/m^3]	2700	2700	
Loss Factor, η	0.001	0.001–1.0	
Thickness, h [mm]	10.0	10.0	

In order to obtain the unknown motions w, u, v, etc., the motions are assumed to be weighted summations of shape functions, ϕ, with weighting factors, q [10]. This definition is given for transverse motion as:

$$w = \sum_{k=1}^{N_s} q_{w,k}(t)\,\phi_{w,k}(x,y) = \mathbf{q}_w^{\mathrm{T}}(t)\,\boldsymbol{\Phi}_w(x,y), \tag{2}$$

where bold terms denote vectors and N_s is the total number of shape functions as well as corresponding vector size. The other motions are defined similarly. Kung and Singh [3] define a minimization scheme whereby the shape functions for all motions can be written in terms of just the transverse shape functions, $\phi_w(x, y)$ and all motions use the same weighting coefficients (i.e. $\mathbf{q}_w = \mathbf{q}_u = \mathbf{q}_v = \mathbf{q}$, etc.) The assumed transverse shape functions ϕ_w are separable and consist of the free-free beam modes, the k^{th} of which is given by:

$$\phi_{w,k}(x,y) = X_m(x)\,Y_n(y), \tag{3}$$

where $X_m(x)$ are given in Fig. 3 for m = 1–3 and $Y_n(y)$ are analogous.

Inserting Eq. 2 and its corresponding companion equations into Eqs. 1a and 1b gives kinetic and potential energy as functions of spatial coordinates x and y, with the weighting vector $\mathbf{q}$ as the N_s unknown terms. Applying Lagrange's equation with respect to the unknown weighting vector to Eqs. 1 results in a system of N_s equations which can be written in matrix form as:

$$\mathbf{M}\ddot{\mathbf{q}} + \mathbf{K}\mathbf{q} = \mathbf{Q}, \tag{4}$$

where $\mathbf{q}$ is the solution vector of weighting coefficients, $\mathbf{M}$ and $\mathbf{K}$ are equivalent mass and stiffness matrices, and $\mathbf{Q}$ is a generalized forcing vector. The equivalent matrices and forcing vector are defined as scaled integrals of the shape functions:

$$\mathbf{M} = \sum_{i=1}^{3} \iint_{A_i} \boldsymbol{\Phi}_i(x,y)\,\mathbf{H}_i\,\boldsymbol{\Phi}_i^{\mathrm{T}}(x,y)\,dxdy, \tag{5a}$$

$$\tilde{\mathbf{K}} = \sum_{i=1}^{3} \iint_{A_i} \left(\mathcal{D}\boldsymbol{\Phi}_i(x,y)\right) \tilde{\mathbf{E}}_i \left(\mathcal{D}\boldsymbol{\Phi}_i(x,y)\right)^{\mathrm{T}} dxdy, \tag{5b}$$

$$\tilde{\mathbf{Q}} = \iint_{A_1} \tilde{F}(x,y)\,\boldsymbol{\Phi}_1(x,y)\,dxdy, \tag{5c}$$

where tildes (~) refer to complex-valued quantities when the loss factor concept is used, i.e. $\tilde{E} = E(1 + j\eta)$, $\mathbf{H}$ and $\mathbf{E}$ are inertia and elasticity matrices, $\mathcal{D}$ is a differential operator (the reader is referred to [3]), and $F(x, y)$ is the spatial distribution of any non-conservative forces on the base layer. These will include a disturbance in the form of a Dirac delta function, or point load, and moments at the patch boundaries [11] as shown in Fig. 1b.

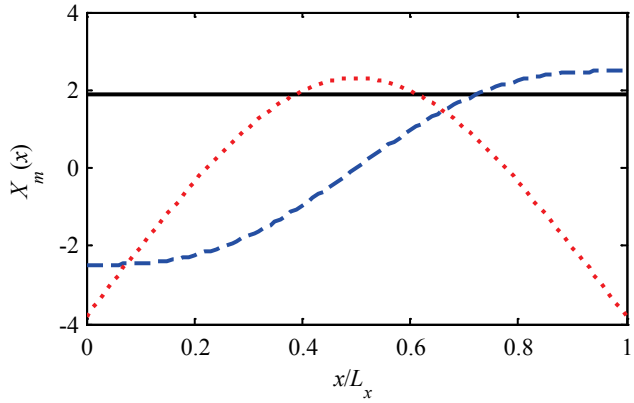

Figure 3. First three transverse shape function in the *x*-direction: *m* = 1 (—), *m* = 2 (- - -), *m* = 3 (···)

From Eq. 4, if steady-state harmonic excitation and response are assumed at frequency ω, $\mathbf{q}$ can be determined as:

$$\tilde{\mathbf{q}} = \left[\tilde{\mathbf{K}} - \omega^2\mathbf{M}\right]^{-1}\left\{\tilde{\mathbf{Q}}_d + \tilde{\mathbf{Q}}_c\right\} \tag{6}$$

and motion $w(x,y)$ can be computed from Eq. 2. Furthermore, natural frequencies (ω_n), modal loss factors (η_n), and mode shapes (w_n) can be determined from the eigenvalues, λ_n, and eigenvectors, Λ_n, of the matrix $[\mathbf{M}^{-1}\mathbf{K}]$ as:

$$\omega_n = \sqrt{\mathrm{Re}\left[\tilde{\lambda}_n\right]}, \tag{7a}$$

$$\eta_n = \mathrm{Im}\left[\tilde{\lambda}_n\right] \Big/ \mathrm{Re}\left[\tilde{\lambda}_n\right], \tag{7b}$$

$$w_n(x,y) = \tilde{\boldsymbol{\Lambda}}_n^{\mathrm{T}}\boldsymbol{\Phi}_w. \tag{7c}$$

4 FORMULATION OF MODEL M2

The continuous system method, M1, has been found to give accurate results in terms of modal loss factors and induced attenuation due to active and passive patches for a thin plate [7]. However, the derivation is somewhat cumbersome and cannot readily give closed-form results for the optimal control effort needed for various cases of passive damping. For this reason, a reduced order (i.e. discretized-system) model is developed to provide insight into the effect of damping on the control effort.

For the sake of simplicity, a traditional beam finite element formulation is used for this model. The beam is discretized into N_e elements of length L_e (such that the beam length $L = N_e \times L_e$), and the endpoints, or nodes, of each element have associated degrees of freedom for transverse motion, w, and slope, θ, as shown in Fig. 4(a). Each node may also have an applied force and/or moment. Slopes and displacements of adjacent elements (common nodes) equate upon assembly, as shown in Fig. 4(b), where node and element numbering scheme is defined. Since free boundaries are used, explicit boundary conditions need not be applied at the first and last nodes.

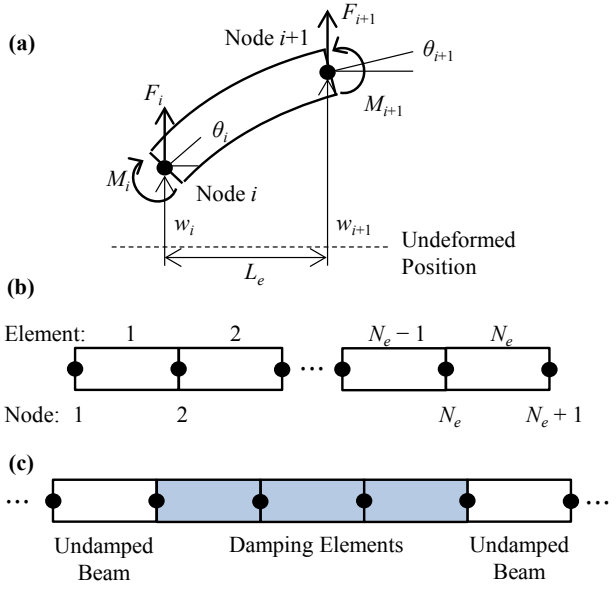

Figure 4. Euler beam finite element formulation: (a) four degrees of freedom of one element; (b) assembled beam elements and numbering convention; (c) assembled elements with equivalent patch elements highlighted in blue

For each element, the four degrees of freedom are placed into an elemental displacement vector, $\mathbf{z}_i^e = \{w_i, \theta_i, w_{i+1}, \theta_{i+1}\}^{\mathrm{T}}$ and the associated elemental mass and stiffness matrices, $\mathbf{M}^e$ and $\mathbf{K}^e$ are given by [12]:

$$\mathbf{M}^e = \frac{\rho b h L_e}{420}\begin{bmatrix} 156 & 22L_e & 54 & -13L_e \\ 22L_e & 4L_e^2 & 13L_e & -3L_e^2 \\ 54 & 13L_e & 156 & -22L_e \\ -13L_e & -3L_e^2 & -22L_e & 4L_e^2 \end{bmatrix}, \tag{8a}$$

$$\mathbf{K}^e = \frac{EI}{L_e^3}\begin{bmatrix} 12 & 6L_e & -12 & 6L_e \\ 6L_e & 4L_e^2 & -6L_e & 2L_e^2 \\ -12 & -6L_e & 12 & -6L_e \\ 6L_e & 2L_e^2 & -6L_e & 4L_e^2 \end{bmatrix}, \tag{8b}$$

where h is beam thickness, b is beam width, and area moment of inertia, $I = bh^3/12$. Global mass and stiffness matrices are assembled as per the standard method [12] and the equations of motion are given in matrix form as:

$$\mathbf{M}\ddot{\mathbf{z}} + \mathbf{K}\mathbf{z} = \mathbf{F}, \tag{9a}$$

$$\mathbf{F} = \{\cdots \quad F_i \quad M_i \quad \cdots\}^{\mathrm{T}}, \tag{9b}$$

$$\mathbf{z} = \{\cdots \quad w_i \quad \theta_i \quad \cdots\}^{\mathrm{T}}, \tag{9c}$$

where matrices are of size $2(N_e+1)$.

For model M2, the passive damping patches are assumed sufficiently compact such that they add only negligible mass, and may therefore be modeled as localized purely damping elements. Effectively, this approximation implies that there is no change in the stored strain energy, Re[U], with the addition of a passive patch. This assumption is valid if the viscoelastic layer has a much smaller shear modulus than the base ($G_2 << G_1$) and the constraining layer is thin ($h_3 < h_1$). There is a further implication that significantly more energy is dissipated by the viscoelastic layer than the base layer, valid for $\eta_2 >> \eta_1$.

In order to implement this approximation, assume that a passive damping patch of length L_p is located at some point, x_p, as in Fig. 5. Define normalized parameters $\bar{x}_p$ and $\bar{L}_p$ as x_p/L and L_p/L respectively, and patch endpoints x_{p2} and x_{p1} as $x_p \pm 0.5L_p$. Parameters $\bar{x}_{p1}$ and $\bar{x}_{p2}$ are similarly normalized by beam length.

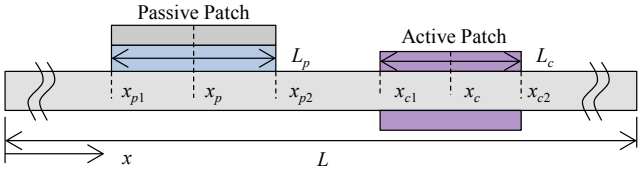

Figure 5. Passive and active patches on a beam with patch endpoints labeled

When assembling the global stiffness matrix, if a majority of the i^{th} element lies within the patch endpoints, that element becomes associated with the passive patch. This can be formalized by the following inequality for the i^{th} element:

$$n_{p1} \le i \le n_{p2} - 1, \tag{10a}$$

$$n_{p1} = \langle \bar{x}_{p1} N_e + 1 \rangle, \quad n_{p2} = \langle \bar{x}_{p2} N_e + 1 \rangle, \tag{10b}$$

where n_{p1} and n_{p2} are the nodes nearest to the patch endpoints and $\langle \cdot \rangle$ denotes the nearest integer (rounding) operator. If both

inequalities in Eq. 10a are satisfied, the beam material Young's modulus, E, should be replaced in Eq. 8b with $\tilde{E} = E\left(1 + j\eta_{eq}\right)$, where η_{eq} is an equivalent loss factor for the damping patch at a given frequency. This is shown schematically in Fig. 4(c), where three elements (highlighted in blue) have complex-valued stiffness and correspond to elements satisfying Eq. 10a.

In model M2, active damping patches are again modeled as point moment inputs to the system on the right-hand side of Eq. 9a. In this case, control moments, M_c and $-M_c$, are inserted at the k^{th} and l^{th} elements, respectively, of $\mathbf{F}$ (from Eq. 9b) where k and l are the indices corresponding to rotation at the nodes nearest to x_{c1} and x_{c2} (from Fig. 6). These nodes can be found similar to Eq. 10b as $n_{c1} = \langle \bar{x}_{c1} N_e + 1 \rangle$ and $n_{c2} = \langle \bar{x}_{c2} N_e + 1 \rangle$.

As with model M1, if harmonic excitation and response are assumed, the governing equation is given by:

$$\tilde{\mathbf{z}} = \left[\tilde{\mathbf{K}} - \omega^2 \mathbf{M}\right]^{-1} \left\{\tilde{\mathbf{F}}_d + \tilde{\mathbf{F}}_d\right\}, \tag{11}$$

and modal properties are the same as those given in Eqs. 7(a) and (b). To obtain the transverse motion of the beam a summation of shape functions is not needed as with M1 (i.e. Eq. 7(c)). Instead the odd elements of the vector $\mathbf{z}$ are extracted into a vector of size N_e+1 giving displacement at each node.

While model M2 loses a degree of dimensionality relative to M1 (1-D beam vs. 2-D plate) this study restricted to an Euler beam so M2 is a reasonable model. Furthermore, M2 supports nodal angular displacement meaning that the model allows for moment input from active patches. Finally, it will be shown in in Section 5 that the required control input can be computed in a more straightforward manner from M2 than from M1.

5 DERIVATION OF REQUIRED CONTROL EFFORT

As mentioned in Section 4, Model M1 has the drawback that the required control effort cannot be readily determined due to the distributed nature of the forcing vector, $\mathbf{Q}$. Model M2, however, is more conducive to this computation since localized point loads correspond to a sparse forcing vector with only as many non-zero elements as there are loads. It is assumed here that the control is independent of system parameters except for the measurement, $\mathbf{z}$.

For the case of M2, first consider "localized" control to reduce the motion of a single node, say w_i, to zero. As the system assumes only a single control parameter (active patch moment input) only a single degree of freedom can be guaranteed to have its motion reduced to zero [13]. First, rewrite Eq. 11, where $\mathbf{A}$ is the system matrix inverse:

$$\tilde{\mathbf{z}} = \left[\tilde{\mathbf{K}} - \omega^2 \mathbf{M}\right]^{-1} \left\{\tilde{\mathbf{F}}_d + \tilde{\mathbf{F}}_c\right\} = \tilde{\mathbf{A}} \left\{\tilde{\mathbf{F}}_d + \tilde{\mathbf{F}}_c\right\}, \tag{12a}$$

$$\begin{Bmatrix} \vdots \\ \tilde{w}_i \\ \vdots \end{Bmatrix} = \begin{bmatrix} \vdots \\ \tilde{\mathbf{A}}_i \\ \vdots \end{bmatrix} \left\{\tilde{\mathbf{F}}_d + \tilde{\mathbf{F}}_c\right\}, \tag{12b}$$

where $\mathbf{A}_i$ is the i^{th} row of the matrix $\mathbf{A}$. However, since $\mathbf{F}_d$ and $\mathbf{F}_c$ have only one and two non-zero elements, respectively (provided there is one disturbance force and one control moment pair), w_i can be written directly as:

$$\tilde{w}_i = \tilde{a}_{ij} \tilde{F}_d + \tilde{a}_{ik} \tilde{M}_c - \tilde{a}_{il} \tilde{M}_c, \tag{13}$$

where a_{ij} is the $(i, j)^{\text{th}}$ element of the matrix $\mathbf{A}$, j is the index of the disturbance force in the vector $\mathbf{F}_d$ (i.e. corresponding to disturbance force location), and k and l are the indices of the control moments in the vector $\mathbf{F}_c$ (i.e. active patch endpoints). A schematic of all nodes of interest is given in Fig. 6.

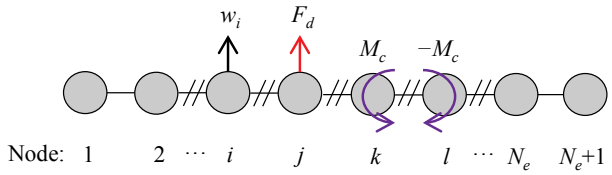

Figure 6. Nodes of interest for inputs and response: *i*: measurement; *j*: disturbance; *k*, *l*: active patch

In order to ensure that w_i is controlled to zero, Eq. 13 implies that the required complex valued control effort must be:

$$\tilde{M}_c = -\tilde{F}_d \frac{\tilde{a}_{ij}}{\tilde{a}_{ik} - \tilde{a}_{il}}. \tag{14}$$

Here, all values come from either the known complex disturbance force or matrix $\mathbf{A}$, which is computed directly from the mass and stiffness matrices.

Similarly, to minimize the global beam motion (i.e. the RMS value or norm of $\mathbf{z}$), first write Eq. 12a as:

$$\tilde{\mathbf{z}} = \begin{bmatrix} \cdots & \tilde{\mathbf{A}}_j & \cdots & \tilde{\mathbf{A}}_k & \cdots \end{bmatrix} \left\{ \begin{matrix} \vdots & \vdots \\ 0 & 0 \\ \tilde{F}_d & 0 \\ 0 & \tilde{M}_c \\ 0 & -\tilde{M}_c \\ \vdots & \vdots \end{matrix} \right\} \begin{matrix} \\ \\ \leftarrow \text{element j} \\ \leftarrow \text{element } k \\ \leftarrow \text{element } l \\ \\ \end{matrix} \tag{15a}$$

$$\tilde{z}_i = \tilde{a}_{ij} \tilde{F}_d + \left(\tilde{a}_{ik} - \tilde{a}_{il}\right) \tilde{M}_c, \tag{15b}$$

where $\mathbf{A}_j$ is the j^{th} column of the matrix $\mathbf{A}$. Again, the compact format of Eq. 15b is facilitated by the sparseness of vectors $\mathbf{F}_d$ and $\mathbf{F}_c$. From here, the norm of $\mathbf{z}$ can be computed and minimized with respect to control effort M_c resulting in:

$$z_{rms} = \left\|\tilde{\mathbf{z}}\right\| = \sqrt{\sum_{i=1}^{2(N_e+1)} \tilde{z}_i \tilde{z}_i^*}, \tag{16a}$$

$$\frac{\partial z_{rms}}{\partial \tilde{M}_c} = 0 \Rightarrow \tilde{M}_c = -\tilde{F}_d \frac{\tilde{\mathbf{A}}_j \cdot \left(\tilde{\mathbf{A}}_k - \tilde{\mathbf{A}}_l\right)^*}{\left(\tilde{\mathbf{A}}_k - \tilde{\mathbf{A}}_l\right) \cdot \left(\tilde{\mathbf{A}}_k - \tilde{\mathbf{A}}_l\right)^*}, \tag{16b}$$

where, again, $\mathbf{A}_j$ is the j^{th} column of the matrix $\mathbf{A}$, • denotes the vector scalar product, and * denotes the complex conjugate. Eq. 16b gives the complex-valued control effort such that the RMS motion of the beam is minimized, resulting in "global" control. It should be noted that while Eqs. 14 and 16 give a compact form of the control parameters, the elements of $\mathbf{A}$ cannot in general be given in closed form as $\mathbf{A}$ is the inverse of the $2(N_e+1) \times 2(N_e+1)$ system matrix.

6 VERIFICATION OF REDUCED ORDER MODEL FOR UNDAMPED BEAM

The reduced order model M2 is compared with results from M1 and the literature to ensure the model is reasonable. First, M2 is verified for an undamped Euler beam in terms of natural frequencies and forced response. Material properties from Table 2 are used for the undamped beam, along with the following geometry: length L = 300 mm, width b = 50 mm, and thickness h = 10 mm. A closed form expression for the n^{th} natural frequency of a free beam [14] is well known as:

$$\omega_n = \sqrt{\frac{EI}{\rho b h}\beta_n^4}, \tag{17}$$

where β_n is a wavenumber that satisfies $\cosh(\beta_n L)\cos(\beta_n L) = 1$ and n is the modal index (where mode n has $n + 1$ nodes or zero crossings). The first three natural frequencies from Model M2 are found to converge rapidly to the result from Eq. 17 with increasing N_e. The case of approximately 50 elements is found to give good accuracy for these modes as well as sufficient spatial resolution for mode shapes. Natural frequencies are also compared between models M1 (with N_s = 64 shape functions), M2 (with N_e = 50 elements) and Eq. 17 in Table 3. For the remainder of this paper, N_s = 64 and N_e = 50 will be used for all verification and case studies. Note that it is expected that M1 provides a larger value of natural frequency than the other methods as the Rayleigh-Ritz method gives an upper bound on frequencies [10].

Table 3. First three beam natural frequencies from three different methods

Mode No.	Model M1*	Model M2	Closed-Form Solution (Eq. 17)
f_1 [Hz]	616	582	572
f_2 [Hz]	1697	1603	1604
f_3 [Hz]	3327	3143	3145

* Model M1 gives additional modes for y-direction participation. Modes listed are those corresponding to beam modes (i.e. plate modes (m, 0))

The forced response of an undamped beam is also computed for driving point accelerance, $\mathcal{A}$ (with $\bar{x}_d = \bar{x}_0 = 1$), defined as transverse acceleration per unit disturbance force:

$$\mathcal{A}(\omega) = -\omega^2 \frac{w(\omega)}{F_d(\omega)}. \tag{18}$$

Figure 7 shows a comparison of models M1 and M2 with a commercial finite element analysis from Abaqus [15]. Note the close agreement between M2 and commercial FEM, verifying the formulation of M2, as well as the upper-bound nature of the natural frequencies determined by M1. Magnitudes agree within a few decibels and the sign of the phases match meaning force and displacement directions are correct.

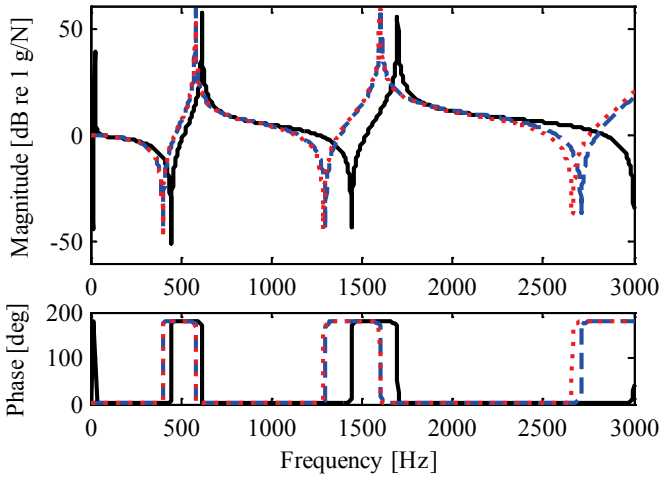

Figure 7. Driving point accelerance of beam: M1 (—), M2 (– –), commercial FEM (···)

7 VERIFICATION OF MODEL M2 WITH PASSIVE PATCH ONLY

Comparisons between M1 (taken to be the benchmark case, as it was validated experimentally in [7]) and M2 are made here to verify results for passive patches. First, take the case of a single passive patch located at $\bar{x}_p$ = 0.5. From previous studies [2, 3] it was shown that constrained layer damping patches induce significant modal damping when the patch is located at points of large strain for that mode. Assuming pure flexure, surface strain is proportional to the curvature, or second derivative of displacement, w_{xx}. This means that for the first flexural mode (i.e. m = 3 from Fig. 3), there is maximum strain at $\bar{x}$ = 0.5 and for the second mode, there is a zero value of strain at $\bar{x}$ = 0.5. Therefore a single patch at this location would suggest significant modal loss factor and attenuation at mode n = 1 and much less damping induced at mode n = 2.

The modal loss factors and broadband responses from M1 and M2 are compared in Fig. 8. Model M1 uses patch size $\bar{L}_p$ = 0.2 and η_2 = 2.0 (from Table 2) M2 uses $\bar{L}_p$ = 0.1 and η_{eq} = 0.05. Forcing is applied at $\bar{x}_d$ = 1 and measurement is $\bar{x}_0$ = 0. Here it is seen that as expected, significant damping is induced at mode 1 but not at mode 2. While different parameters are

used here (there is a complicated relationship between η_2 from M1 and η_{eq} from M2), it can be seen that similar trends as predicted (and validated) by M1 are given by M2. Reasonable agreement in insertion loss is seen at both modes (which is dependent on frequency resolution) and excellent agreement in loss factor is observed. Note that M1 predicts a slight frequency shift with the presence of passive patches (an actual phenomenon due to mass loading and stiffness modification) whereas M2, which only models the effective loss factor and neglects change to the mass matrix, does not.

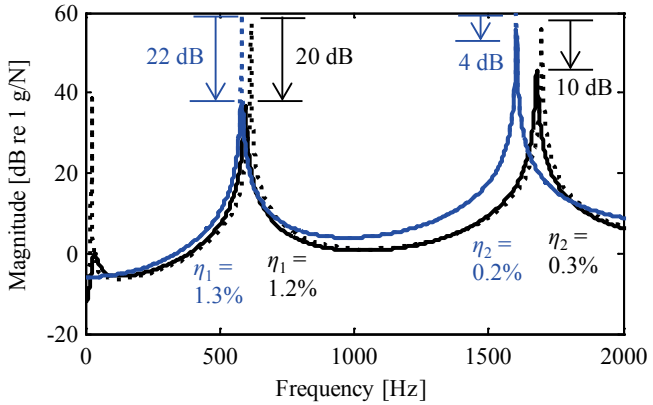

Figure 8. Cross point accelerance magnitude: undamped (⋯), one passive patch (—), M1 (black), M2 (blue)

To further verify the modeling of passive patches with M2, a location dependence study is performed. In this study, the first three modal loss factors are computed for a beam with a single patch of size $\bar{L}_p = 0.1$, $\eta_{eq} = 0.5$, and location varying from $\bar{x}_p = 0.05$ to 0.95. Results are plotted in Fig. 9. As expected the highest corresponding modal loss factors occur when $\bar{L}_p$ is at a point of maximum strain or curvature for each mode. The "jaggedness" on some areas of the curves in Fig. 9 is a result of the discretized nature M2; the patch location cannot be smoothly varied as satisfaction of the inequality in Eq. 10a occurs at discrete intervals. However with increased number of elements the smoothness of the curves increases.

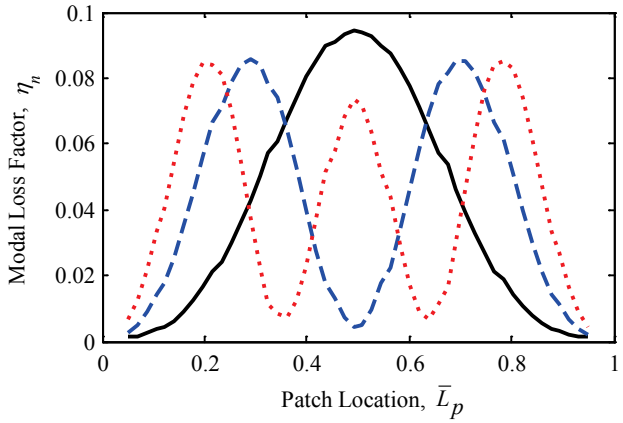

Figure 9. Passive patch location dependence study: mode $n = 1$ (—), $n = 2$ (– –), $n = 3$ (⋯)

8 VERIFICATION OF MODEL M2 WITH ACTIVE PATCH CONTROL EFFORT

The calculated control efforts of Eqs. 14 and 16b are verified to ensure local and global control are implemented as expected. First the beam is excited by a harmonic disturbance force (1 N ∠0°) at its first flexural mode. Figure 10(a) shows the response, in particular of the measurement location ($\bar{x}_0 = 0$), to be approximately 0.6 mm peak-to-peak. When an active patch is applied with the local control effort of Eq. 14 (along with a passive patch at $\bar{x}_p = 0.6$), the resulting response is shown in Fig. 10(b) to be three orders of magnitude smaller and with zero displacement at the measurement location. Equation 14 computes the required control effort for this case to be 0.117 N-m ∠−1.8°.

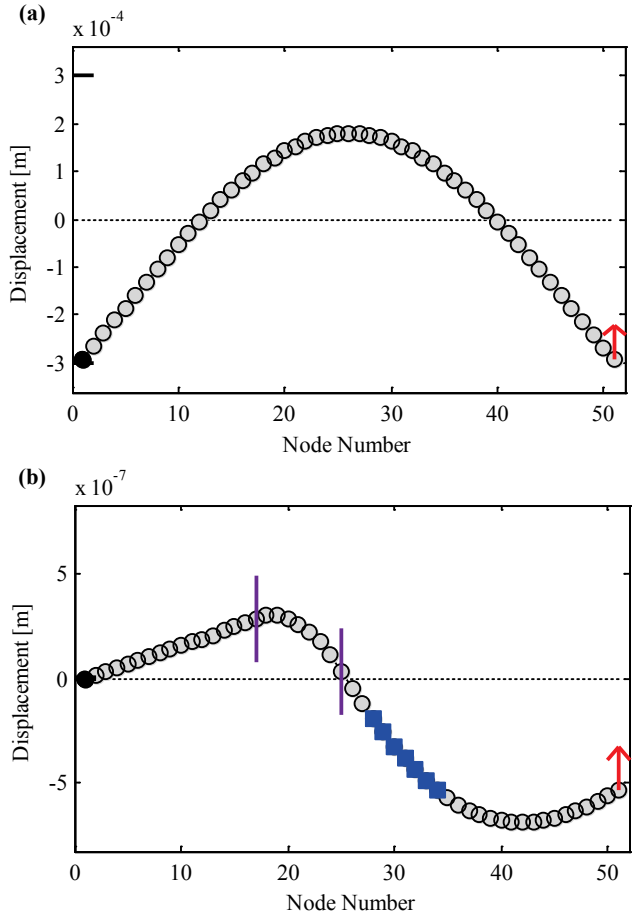

Figure 10. Local control verification with model M2: (a) beam with no patches; (b) beam with active and passive patches subject to control at $x_0 = 0$, disturbance force (↑), active patch control moment (|), passive patch (■), measurement location (●)

Next the global control effort of Eq. 16b is verified. For the same conditions described in the previous exercise, Eq. 16b computes the optimal control effort to be 0.117 N-m ∠−2.1°. This control value is adjusted in terms of its phase (by ±180°) at constant magnitude and its magnitude (by a factor of 0.1–10)

at constant phase. The RMS response, $z_{rms} = \|\mathbf{z}\|$ is computed for each case, and results are shown in Figs. 11(a) and 11(b).

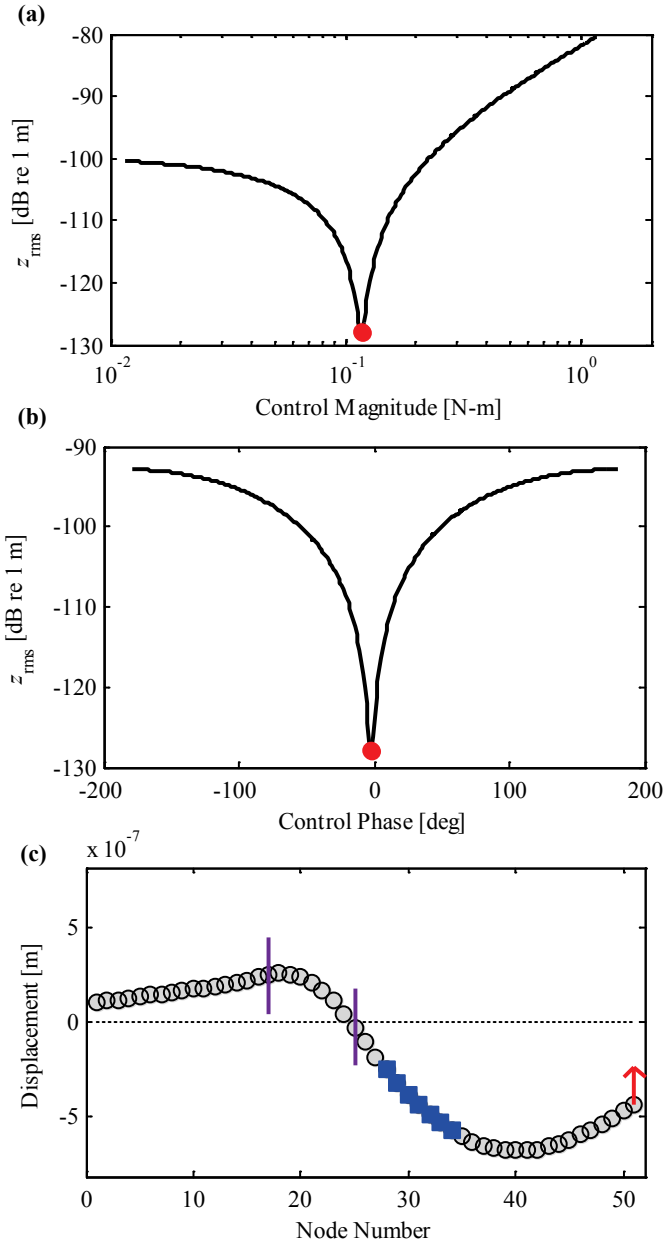

Figure 11. Global control verification study with model M2: (a) varying magnitude at constant phase (—), optimal value from Eq. 16b (•); (b) varying phase at constant magnitude; (c) controlled displacement shape

Here it is seen that in both cases the optimal control effort from Eq. 16b minimizes the RMS motion. Figure 11(c) shows the displacement shape of the beam under global control. Note that node 1 at $\bar{x}_0 = 0$ no longer has zero displacement, but instead the global displacement (z_{rms}) is slightly reduced (0.405 μm rather than 0.414 μm).

9 ILLUSTRATIVE CASE STUDIES WITH MODEL M2

Next, two case studies are presented that demonstrate the utility of M2 for rapid investigation of parametric changes. The first case study (termed as Study A) will be the effect of the passive damping patch relative to the inputs and measurement (for local control) at the second flexural mode. Cases 1 and 2 are defined in Fig. 12, where Case 1 puts the passive patch between the inputs and the measurement and Case 2 puts the passive patch between the disturbance and control.

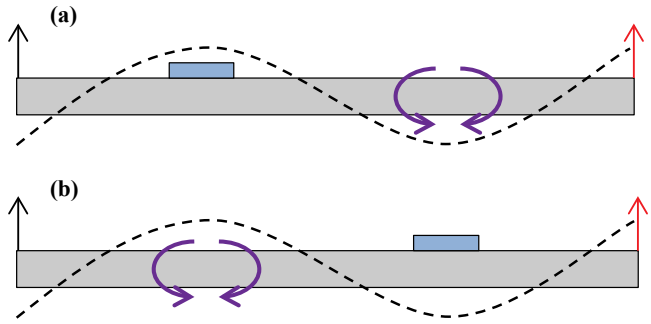

Figure 12. Effect of passive patch location relative to active control for mode $n = 2$: (a) Case A1; (b) Case A2

In this study, all locations and patch sizes ($\bar{L}_p = 0.2$, $\bar{L}_c = 0.1$) are fixed and η_{eq} is varied from 0.001 to 1.0. Results in terms of the RMS beam motion and control effort are shown in Table 4 and Fig. 13.

Table 4. Changes in parameters and response with increasing η_{eq} for Study A

Case	Control Mag. [N-m/N]	Control Phase [deg]	RMS Motion [μm]
A1	0.067	0 to 1	0.070 to 0.062
A2	0.069	−180 to −165	0.105 to 0.094

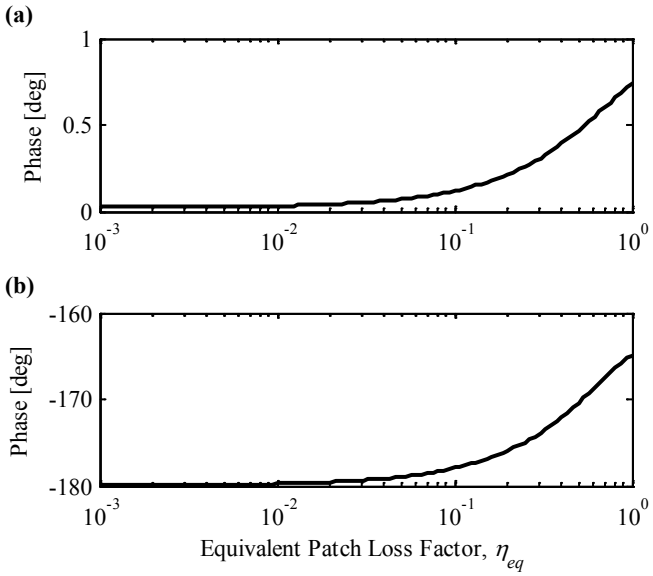

Figure 13. Effect of a change in equivalent loss factor on control phase: (a) Case A1; (b) Case A2

The increase in η_{eq} has negligible effect on most of the parameters except for the control phase in Case 2 (Fig. 13(b)), which is shifted by about 15° by the presence of large η_{eq}. Here it is seen that the location of the passive patch has an important influence on the complex control effort, especially in the case of high damping. It is also seen that Case 1 results in lower RMS motion, perhaps suggesting that control and disturbance distributed across the structure reduces global motions.

Next local vs. global control is studied (termed Study B). Here all locations and patch sizes are fixed as in the case A2, but B1 invokes local control whereas B2 uses global control. The results from this study are detailed in Table 5. When implementing global control, the change to the control phase is significantly reduced (shown in Fig. 14(b)) as compared to local control. The control magnitude is largely unchanged and the RMS motion is reduced by 5 to 10%, depending on damping. From this study, it can be ascertained that if local control of a single node is not required, global control may result in a simpler control effort with less global motion.

Table 5. Changes in parameters and response with increasing η_{eq} for Study B

Case	Control Mag. [N-m/N]	Control Phase [deg]	RMS Motion [μm]
B1	0.069	−180 to −165	0.105 to 0.094
B2	0.069	−180 to −178	0.096 to 0.085

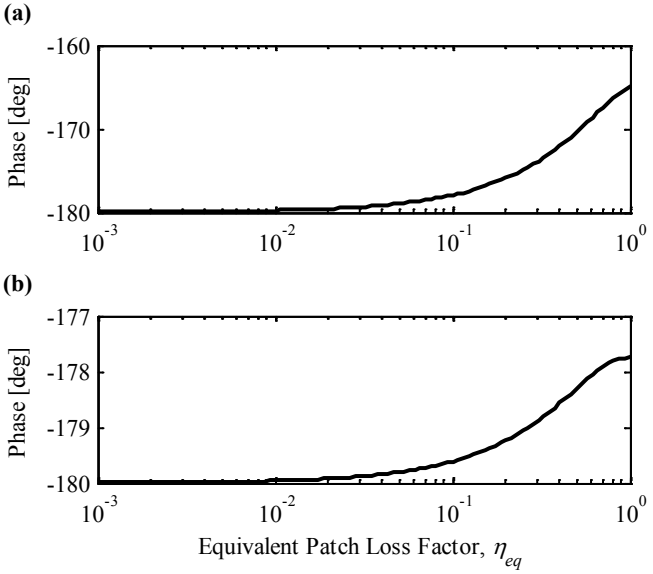

Figure 14. Effect of a change in equivalent loss factor on control phase: (a) Case B1; (b) Case B2

10 CONCLUSION

This paper presents a simplified and reduced-order finite element model for the vibratory analysis of an Euler beam with combined active and passive damping patches. This approximation, termed M2, is compared with benchmark model M1 for validation. Reasonable agreement is seen in terms of the natural frequency, modal loss factor, and forced response, especially in terms of trends observed with passive patch size and location. Model M2 has the benefit that the control effort for both localized and global motion reduction can be computed compactly and easily as compared with M1; thus M2 is more conducive to parametric design studies.

Illustrative examples of potential case studies are presented in the paper. For example M2 could be used to quickly find the effect of patch size, location, and equivalent loss factor on the control effort and local/global response of the beam. Perhaps more interesting are studies that involve the effect of the placement of patches, disturbance, and measurement relative to a given mode shape. Any such studies could be carried out efficiently for either control law. Future work with this model could include the effects of multiple patches, unsteady time-domain analysis, and extension of model M2 to a thin plate. As the method of concurrent active and passive damping patches is still developing, it is important to have a variety of analysis tools to determine the effects of different structures and patch configurations. While the model presented in this paper is simplified and cannot predict exact results, it permits rapid investigation of the physics of these problems. Furthermore, the model can provide valuable insight when used in conjunction with traditional methods such as analytical formulations (e.g. model M1) and large-scale commercial computational codes.

ACKNOWLEDGMENTS

The authors would like to acknowledge the OSU Graduate School, the Ohio Space Grant Consortium, the Smart Vehicle Concepts Center (www.SmartVehicleCenter.org), and the National Science Foundation Industry/University Cooperative Research Centers program (www.nsf.gov/eng/iip/iucrc) for funding this work through graduate fellowships and financial assistance.

REFERENCES

[1] Benjeddou, A., 2001, "Advances in Hybrid Active-Passive Vibration and Noise Control via Piezoelectric and Viscoelastic Constrained Layer Treatments," Journal of Vibration and Control, 7, pp. 565–602.

[2] Kung, S. W. and Singh, R., 1998, "Vibration Analysis of Beams with Multiple Constrained Layer Damping Patches," Journal of Sound and Vibration, 212(5), pp. 781–805.

[3] Kung, S. W. and Singh, R., 1998, "Complex Eigensolutions of Rectangular Plates with Damping Patches," Journal of Sound and Vibration, 216(1), pp. 1–28.

[4] Clark, R. L., Fuller, C. R., and Wicks, A., 1991, "Characterization of Multiple Piezoelectric Actuators for Structural Excitation," Journal of the Acoustical Society of America, 90(1), pp. 346–357.

[5] Dimitriadis, E. K., Fuller, C. R., and Rogers, C. A., 1991, "Piezoelectric Actuators for Distributed Vibration Excitation of Thin Plates," Journal of Vibration and Acoustics, 113, pp. 100–107

[6] Lam, M. J., Inman, D. J., and Saunders, W. R., 1997, "Vibration Control through Passive Constrained Layer

Damping and Active Control," J. Intelligent Material Systems and Structures, 8, pp. 663–677.
[7] Plattenburg, J., Dreyer, J. T., and Singh, R., 2015, "Active and Passive Damping Patches on a Thin Rectangular Plate: A Refined Analytical Model with Experimental Validation," Journal of Sound and Vibration, 353, pp. 75–95.
[8] Kumar, K. R. and Narayanan, S., 2008, "Active Vibration Control of Beams with Optimal Placement of Piezoelectric Sensor/Actuator Pairs," Smart Materials and Structures, 17, pp. 1–15.
[9] Soedel, W., 2004, Vibrations of Plates and Shells, Marcel Dekker, New York, Chap. 7.
[10] Meirovitch, L., 2001, Fundamentals of Vibrations, McGraw Hill, New York, Chap. 9.
[11] Crawley, E. F., and de Luis, J., 1987, "Use of Piezoelectric Actuators as Elements of Intelligent Control Structures," American Institute of Aeronautics and Astronautics Journal, 25(10), pp. 1373–1385.
[12] Przemieniecki, J. S., 1968, Theory of Matrix Structural Analysis, McGraw Hill, New York, Chap. 10.
[13] Antsaklis, P. J., and Michel, A. N., 2007, A Linear Systems Primer, Birkhauser, Boston, MA, Chap. 5.
[14] Hartog, J. P. Den, 1985, Mechanical Vibrations, Dover Publications, New York, Appendix V.
[15] Abaqus Ver. 6.13, <http://www.3ds.com/products-services/simulia/portfolio/abaqus/overview/>

APPENDIX A: LIST OF SYMBOLS

A	plate or patch area
$\mathbf{A}$	system matrix (inverted)
a	element of system matrix
$\mathcal{A}$	accelerance
b	beam width
E	Young's modulus
F	force
$\mathbf{F}$	finite element forcing vector
f	frequency
G	shear modulus
h	beam thickness
I	area moment of interia
i	counting index
j	imaginary number, $\sqrt{-1}$
K	kinetic energy
$\mathbf{K}$	stiffness matrix
L	beam length
M	moment
$\mathbf{M}$	mass matrix
N	number (of shape functions, elements)
n	node number
$\mathbf{Q}$	generalized forcing vector
$\mathbf{q}$	shape function weighting vector
T	kinetic energy
U	potential energy
u, v	in-plane displacement
w	transverse displacement
x, y, z	spatial coordinates
$\mathbf{z}$	finite element generalized displacement vector
β	wavenumber
γ	shear strain
η	loss factor
θ	element rotation
$\mathbf{\Lambda}$	eigenvector
λ	eigenvalue
ν	Poisson's ratio
ρ	mass density per unit volume
$\mathbf{\Phi}$	shape function vector
ϕ	shape function
ω	angular frequency

Subscripts

c	control
d	disturbance
e	element (FEM)
eq	equivalent loss factor for passive patch
i, j, k, l	matrix indices (for locations of measurement, disturbance, and control)
m, n	modal indices
p	passive patch
s	shape function
x, y	spatial partial derivatives
1, 2, 3	layers in analytical formulation

Superscripts

e	elemental matrix (FEM)
$\tilde{}$	complex-valued
$\bar{}$	normalized quantity (overbar)

Operators

$\mathcal{D}$	spatial differential operator for matrices
Im	imaginary part of complex number
Re	real part of complex number
$\angle$	angle of complex number
$\langle\cdot\rangle$	nearest integer
$\bullet$	vector scalar product
$\|\cdot\|$	matrix norm
T	matrix transpose
*	complex conjugate

